ACS APPLIED MATERIALS

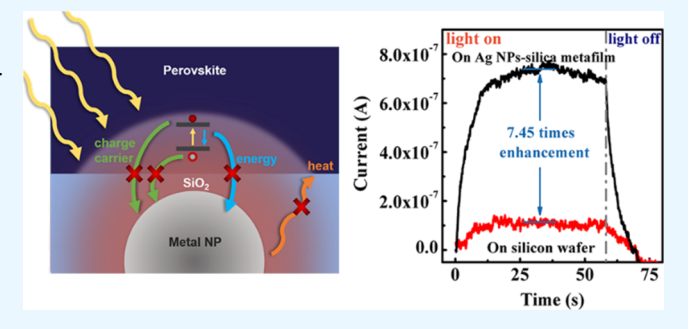
Using Silver Nanoparticles-Embedded Silica Metafilms as Substrates to Enhance the Performance of Perovskite Photodetectors

♦ Cite This: ACS Appl. Mater. Interfaces 2019, 11, 32301−32309

Bo Liu,*^{,†} Rithvik R. Gutha,[‡] Bhupal Kattel,[†] Mohammed Alamri,[†] Maogang Gong,[†] Seyed M. Sadeghi, ** Wai-Lun Chan, ** and Judy Z. Wu*, **

Supporting Information

ABSTRACT: Plasmonic metal nanostructures provide a promising strategy for light trapping and therefore can dramatically enhance photocurrent in optoelectronics only if the trapped light can be coupled effectively from plasmons to excitons, whereas the reverse transfer of energy, charge, and heat from excitons to plasmons can be suppressed. Motivated by this, this work develops a scheme to implement a metafilm with Ag nanoparticles (NPs) embedded in 10 nm thick silica (Ag NPs-silica metafilm) to the active device channel of a hybrid perovskite film/graphene photodetector. Remarkably, an enhancement factor of 7.45 in photoresponsivity, the



highest so far among all the reports adopting plasmonic metal NPs in perovskite photodetectors, has been achieved on the photodetectors with the Ag NPs-silica metafilms. Considering that the synthesis of the Ag NPs-silica metafilms can be readily scaled up to coat both rigid and flexible substrates, this result provides a low-cost metaplatform for a variety of high-performance optoelectronic device applications.

KEYWORDS: perovskite, photodetectors, plasmonic effect, metal nanoparticles, metafilms

1. INTRODUCTION

Organic-inorganic hybrid perovskite thin films with a typical form of CH₃NH₃PbX₃ (X = Cl, Br, or I) have been broadly utilized in optoelectronic devices including photovoltaics, light-emitting diodes, 3,4 and photodetectors 5-7 over the recent few years because of the combination of several unique merits of the perovskites including direct band gaps tunable in the visible spectrum, high light absorption coefficients up to 1.5 × 10⁴ cm⁻¹, and long-range electron and hole diffusion lengths on the order of micrometers. A perovskite/graphene heterojunction is formed by stacking a perovskite film on graphene. The built-in electric field across the perovskite/ graphene interface because of their band edge alignment often facilitates transfer of the photogenerated charge carriers from perovskite to graphene. The high charge mobility in graphene for charge transport can therefore lead to the high photoconductive gain and enhanced photoresponsivity that have been achieved in perovskite/graphene heterojunction photodetectors. 10-16 Compared to the vertical structured perovskite photodetectors without graphene which have responsivity typically in the range of a few micro-amperes per watt to several amperes per watt, 17-19 the perovskite film/graphene heterojunction photodetectors can have much higher photoresponsivity. For example, Lee et al. reported responsivity of 180 A/W at the wavelength of 520 nm on perovskite film/ graphene heterojunction photodetectors. 13 Dang et al.

fabricated a perovskite film/graphene heterojunction photodetector on a flexible substrate and obtained a maximum responsivity of 115 A/W under 515 nm light illumination. 10 Applying microfabrication techniques in devices fabrication to obtain optimal graphene channel dimension and hence higher photoconductive grain, responsivity up to $\sim 10^6$ A/W has been demonstrated on perovskite/graphene heterojunction photodetectors based on both perovskite films 16 and perovskite nanocrystals.11

Achieving higher photoresponsivity is important to highperformance photodetectors. This can be achieved through enhanced light absorption of perovskite thin films or nanocrystals using plasmonic nanostructures for light trapping. Metal nanoparticles (NPs) have been extensively adopted for light management in the visible spectrum. 20-22 On metal NPs, localized surface plasmon resonance (LSPR) can be excited by incident lights and a strong evanescent electromagnetic (EM) field can be generated around the metal NPs within a short range of a few tens to a few hundreds of nanometers. 23,24 The LSPR frequency is determined by free electron concentration in the metal, with minor tunability by the size and shape of the metal NPs as well as the external surrounding media.²⁵ An

Received: June 18, 2019 Accepted: August 12, 2019 Published: August 22, 2019

Department of Physics and Astronomy, The University of Kansas, Lawrence, Kansas 66045, United States

^{*}Department of Physics and Astronomy, The University of Alabama in Huntsville, Huntsville, Alabama 35899, United States

ACS Applied Materials & Interfaces

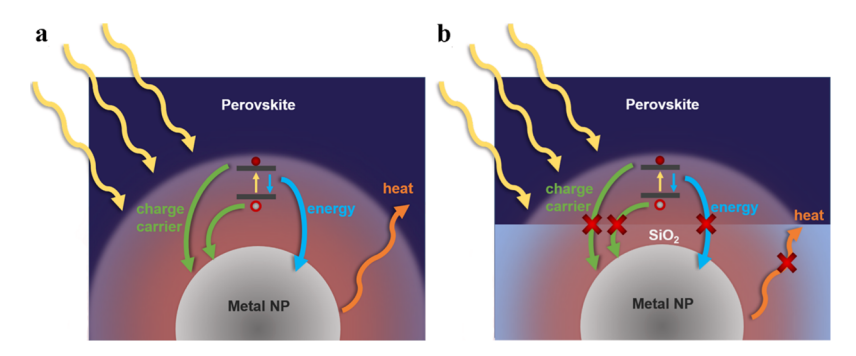


Figure 1. Schematic diagrams of a (a) metal NP embedded in a perovskite thin film with a direct contact to perovskite and a (b) metal NP embedded in a SiO₂ metafilm with a perovskite thin film atop. The yellow arrows represent incident light on the perovskite. The charge, energy, and heat transfer effects are illustrated by green, blue, and orange arrows, respectively, which can be effectively suppressed using the Ag NPembedded silica metafilm as depicted in (b).

important result of the LSPR is the enhancement of EM field surrounding metal NPs from several times to tens of times. 25-27 Therefore, this enhanced EM field can provide dramatically enhanced absorption to the photosensitizer layer, leading to an increased concentration of electron-hole pairs and thereby improved photoresponsivity. Typically, Ag and Au are two promising plasmonic materials for the application in the perovskite photodetector, as the LSPR frequency of Ag and Au could be tuned over the visible spectrum²⁸ that matches the absorption spectrum of perovskite thin films.

A few groups have reported moderately enhanced photoresponsivity on perovskite thin film photodetectors by implementing plasmonic metal NPs in the device. Sun et al. reported enhanced responsivity by a factor of 1.96 on perovskite (400 nm thick)/graphene heterojunction photodetectors by embedding plasmonic Au NPs of ~40 nm diameter directly underneath graphene.²⁹ Wang et al. improved the photoresponsivity of a vertical structured perovskite photodetector by 59% by inserting Au nanorods in the perovskite layer.³⁰ These early studies generally merged metal NPs in the device with direct contact to the perovskite film, which leads to, however, several drawbacks that counteract the benefits of NPs plasmonic optical enhancement. First, the natural defect sites on the surface of metal NPs could trap both electron and holes excited in the perovskite layer, increasing the recombination of the photogenerated charge carriers.³¹ On the other hand, surface energy transfer could take place, in which photoexcited electrons recombine with the holes in perovskite and transfer the excitation energy to the neighboring metal NPs. 32,33 Both charge and energy transfers between perovskite and metal NPs cause the significant loss of photogenerated charge carriers in perovskite, thus strongly weakening the plasmonic enhancement as a consequence. Finally, an additional problem of the direct contact between perovskite and metal NPs is that the heat resulted from decay of plasmons³⁴ in metal NPs could induce structural and chemical changes³⁵ in perovskite, thereby degrading the device performance. To minimize all the issues discussed above, integrating plasmonic metal NPs into perovskite photodetectors must be deliberately designed in order to achieve optimal responsivity enhancement.

In this work, we report a new device structure by implementing an Ag NPs-embedded SiO₂ (Ag NPs-silica) metafilm as the substrate of the perovskite/graphene photodetector, aiming at efficiently availing plasmonic enhancement by suppressing unfavorable charge, energy, and heat transfers.

Considering the instability of the metafilms under the thermal budgets required for fabrication of the perovskite/graphene photodetectors, which can typically cause short-circuits of the devices because of thermally driven metal diffusion from metal NPs to the surface of the SiO₂ overlayer, the metafilm was precisely fabricated under the active photodetector channel defined between the Au electrodes. This allows for successful plasmonic metafilm optical enhancement, for the first time to our knowledge, in an optoelectronic device. Specifically, an enhancement factor of 7.45 in the responsivity was obtained in the perovskite/graphene photodetector on the Ag NPs-silica metafilm as compared to the counterpart without Ag NPs integration, which is the highest so far among all the reports adopting the strategy of integrating plasmonic NPs in perovskite photodetectors.

2. RESULTS AND DISCUSSION

Figure 1 illustrates schematically the difference in plasmonexciton coupling when the Ag NPs are in contact with the perovskite film, Figure 1a, and are separated by a 10 nm thick SiO₂ layer, Figure 1b. The green, blue, and orange arrows in Figure 1a represent the charge, surface energy, and heat transfer, respectively; all can cause a significant loss of photogenerated charge carriers in perovskite, thus strongly weakening the plasmonic enhancement as the consequence. As illustrated in Figure 1b, a 10 nm SiO₂ overlayer is designed to suppress charge, energy, and heat transfers between the perovskite film and Ag NPs in this work while still allowing the perovskite sensitizer to take the advantage of the plasmonic light trapping enhanced EM field. The suppression of the charge and energy transfers using a dielectric passivation layer of optimal thickness of 10-15 nm has been demonstrated in the enhanced emission of CdSe/ZnS quantum dots (QDs) on the plasmonic Au film coated with a SiO₂ layer. ^{36,37} Additionally, the SiO₂ layer is expected to considerably reduce heat transfer from Ag NPs to perovskite and therefore could effectively protect the perovskite film from heat-induced degradation.

Figure 2a depicts the three-dimensional schematic illustration and cross-sectional view of the perovskite/graphene heterojunction photodetector on an Ag NPs-silica metafilm substrate designed in this work. In order to avoid short-circuits, the metafilm was precisely fabricated under the active channel of the perovskite/graphene heterojunction photodetectors (see details of the device fabrication in Methods). Organicinorganic hybrid perovskite CH₃NH₃PbI₃ films were deposited

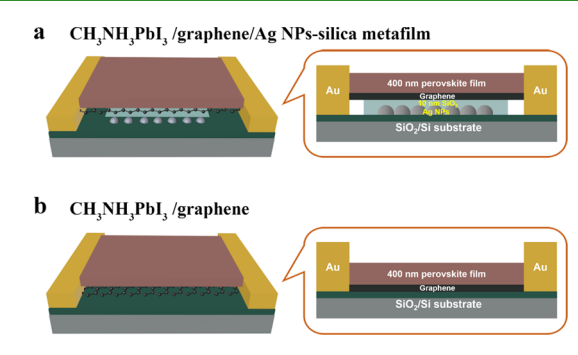


Figure 2. Schematic structure of a (a) perovskite/graphene heterojunction photodetector on the Ag NPs-silica metafilm; Ag NPs were located within the graphene channel region; and (b) perovskite/graphene heterojunction photodetector without the Ag NPs-silica metafilm.

on top of the graphene, with two Au electrodes defining the region of the active device channel. Underneath the graphene channel, Ag NPs were embedded in a 10 nm thick SiO₂ layer. The LSPR on the embedded Ag NPs is induced by the unabsorbed part of the incident light on the device and produces a strongly enhanced evanescent EM field, which can significantly enhance the absorption of the perovskite. The 10 nm thick SiO₂ superstrate layer isolates the underneath Ag NPs from the perovskite layer to suppress the detrimental charge and energy transfers from perovskite to Ag NPs for optimal plasmonic light trapping. Meanwhile, the SiO2 layer can also prevent surface contamination of the Ag NPs via air/chemical exposure and silver iodide formation³⁸ from the subsequent steps of graphene transfer and perovskite film fabrication. A perovskite photodetector without Ag NPs-silica metafilm substrate is shown in Figure 2b for comparison purposes in this

Figure 3a shows a scanning electron microscopy (SEM) image of the Ag NPs fabricated on a SiO₂/Si substrate (see Methods for Ag NP fabrication details). Hemispheric Ag NPs formed after the thermal annealing.³⁹ The size distribution of Ag NPs can be estimated from the SEM image using ImageTool. Four 0.5 μ m \times 0.5 μ m squares were chosen randomly from the SEM scanned region and the diameters of the Ag NPs in each square were measured and the result is depicted in Figure 3b. The lateral dimension of the Ag NPs is 58.64 ± 28.07 nm. Although a better uniformity of the Ag NP dimension could be obtained by controlling the post annealing condition to achieve a narrower band LSPR, 40 a broader band LSPR in this work is favorable in the perovskite/graphene heterojunction devices that aim to cover almost the entire visible spectrum.

Figure 3c shows the absorption spectra of Ag NPs fabricated on glass without (blue) and with (red) the 10 nm SiO₂ layer. An LSPR peak of the Ag NPs can be observed at the wavelength of 490 nm in the former. The 10 nm SiO₂ superstrate on the Ag NPs shifts the LSPR peak to ~585 nm and this red shift is ascribed to the effect of higher dielectric constant of SiO₂ as compared to that of air. ^{28,41} Meanwhile, the plasmonic peaks are found to be broad, which are originated from the broad size distribution of Ag NPs in the range of 20-90 nm as the resonance wavelength (or frequency) is also related to the size of NPs^{24,41} and will have a more red shift when the size becomes larger.²⁵ The broad peak indicates that the LSPR could be induced by a wide range of wavelength across the visible spectrum in which the perovskite is active.

Figure 3d compares the Raman spectra of single-layer graphene on a Si substrate and graphene on a SiO₂ (10 nm)/ Ag NPs/Si substrate taken with a 532 nm laser. The two characteristic peaks correspond to G (at 1585 cm⁻¹) and 2D bands at (2668 cm⁻¹). The G band is associated to the primary

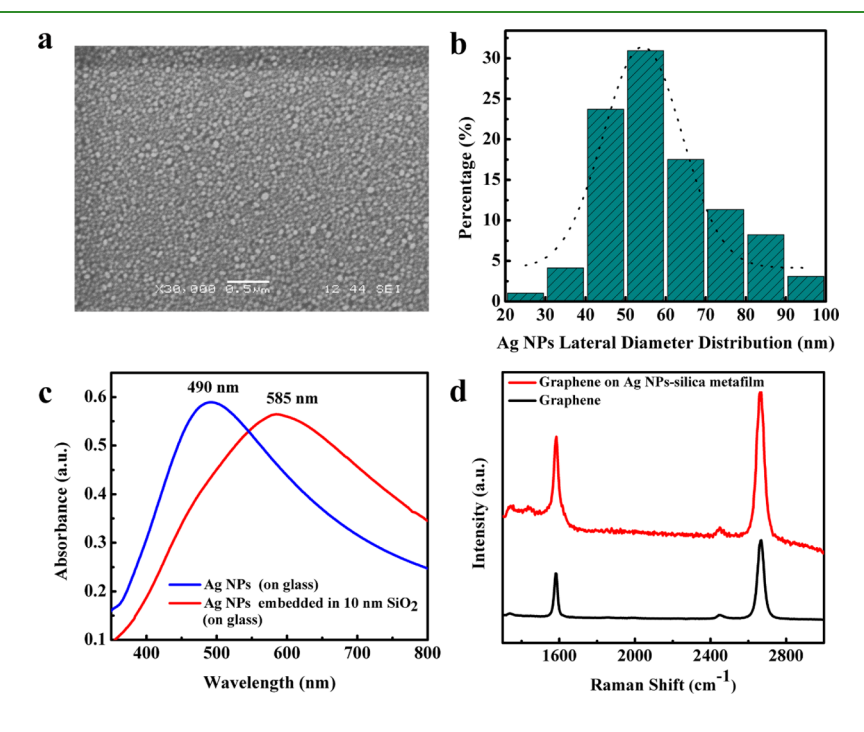


Figure 3. (a) SEM image of Ag NPs on SiO₂/Si; (b) lateral diameter distribution of the Ag NPs; (c) absorption spectrum of Ag NPs/glass substrate without (blue) and with (red) a 10 nm SiO2 superstrate layer. The nominal thickness of the Ag NPs is 8 nm; and (d) Raman spectra of graphene on a SiO₂/Si (black) substrate and on a Ag NPs-silica metafilm substrate (red).

ACS Applied Materials & Interfaces

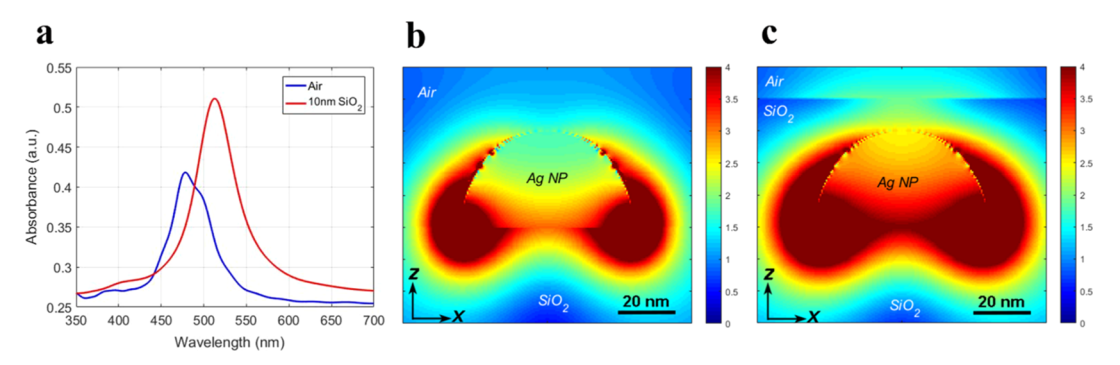


Figure 4. (a) Simulation absorption spectrum of Ag NPs of 60 nm diameter without (blue) and with (red) a 10 nm thick SiO₂ superstrate; mode profile of the Ag NP without (b) and with (c) a 10 nm SiO₂ superstrate at the resonant wavelength along the xz-plane.

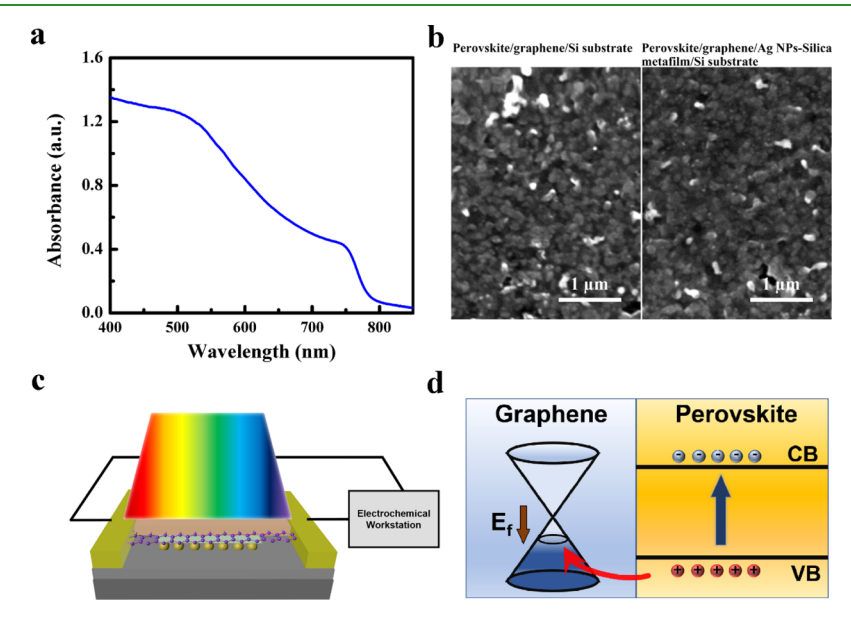


Figure 5. (a) Absorption spectrum of 400 nm thick perovskite film deposited on glass using the same fabrication process for perovskite/graphene photodetectors; (b) SEM images of a perovskite film fabricated on a graphene/Si substrate (left) and on a graphene/Ag NPs-silica metafilm/Si substrate (right); (c) experimental setup for photoresponse measurement; (d) illustration of the perovskite/graphene interface energy band alignment.

in-plane vibrational mode and the 2D band is the second order of the D band (at 1356 cm⁻¹) that corresponds to the A_{1g} breathing mode of the hexagonal rings. The ratio of the 2D and G band intensities $(I_{\rm 2D}/I_{\rm G})$ of ~1.8 and the negligible intensity of the D peak of pristine graphene indicates that the graphene is a single layer with low concentration of defects.⁴² The intensities of the G and 2D peaks of graphene on Ag NPs are enhanced by a factor of ~2 because of the LSPR enhancement by Ag NPs on graphene. 43 This enhancement factor is comparable to the values of 1.3 and 1.8 for graphene with Ag NPs of 8 and 14 nm nominal thicknesses, respectively.³⁹ The ratio of the 2D and G peak intensities is slightly suppressed $(I_{2D}/I_G \approx 1.5)$ because of the different enhancement factors for 2D and G peaks of graphene on Ag NPs.⁴⁴

To study the impact of the Ag NPs on the enhancement of responsivity of the photodetector, we simulated the interaction of light with Ag NPs with a diameter of 60 nm to replicate the fabricated sample as closely as possible using the Lumerical Finite-Difference Time-Domain (FDTD) solutions software. A plane wave was selected with the illumination axis being along the z-axis (downward from the top of the Ag NP). Figure 4a shows the calculated absorbance spectra of such an Ag NP with and without the 10 nm SiO₂ superstrate, which agree

qualitatively with the experiment (Figure 3c) except that the resonance peak is narrower and the LSPR peak red shift is smaller on addition of the 10 nm SiO₂ superstrate. These discrepancies may be associated with the broad size distribution and nonuniform shape of the Ag NPs in the experimental sample. An additional difference is in the SiO₂ configuration employed in the simulation for simplicity that the Ag NP is embedded in the SiO₂ of a much larger thickness except for maintaining the thickness of the SiO2 at 10 nm at the very top of the Ag NP as shown in Figure 4c. This differs from the experimental configuration of the 10 nm thick SiO₂ layer coated around the top side of the Ag NPs. Figure 4b,c compares the simulated mode profiles around an Ag NP without and with the 10 nm SiO₂ superstrate. The results show the significant impact of the SiO₂ layer on enhancement of plasmonic fields of the Ag NP, particularly along the z-axis above the SiO₂ layer. The plasmonic field on top of the Ag NP penetrates the air and has at least two times field enhancement, or power of the light field at least four times, with a penetration depth of a few nanometers. Replacing the air with perovskite (higher dielectric constant) would increase the field enhancement factor further. Furthermore, the field enhancement factor should be considerably higher if considering the contributions **ACS Applied Materials & Interfaces**

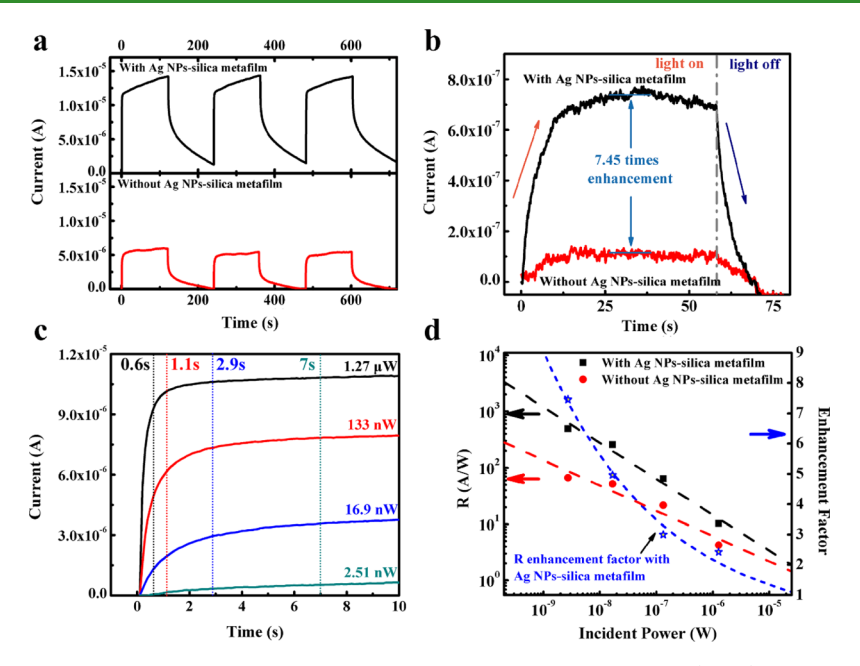


Figure 6. (a) Dynamic photoresponse of perovskite/graphene heterojunction photodetectors with (black) and without (red) a Ag NPs-silica metafilm under 585 nm illumination, $P_{\rm in} = 1.27 \times 10^{-6}$ W, bias = 0.1 V; (b) amplified view of one cycle of photoresponse of perovskite/graphene heterojunction photodetectors with (black) and without (red) a Ag NPs-silica metafilm under 585 nm illumination, $P_{in} = 2.51 \times 10^{-9}$ W, bias = 0.1 V; (c) comparison of the response time (rise time) of the devices on the Ag-silica metafilms under different incident light power; (d) photoresponsivity vs incident power of perovskite photodetectors with (black) and without (red) a Ag NPs-silica metafilm under 585 nm illumination, and bias voltage of 0.1 V; the blue stars represent the enhancement factor of the photoresponsivity and blue dashed curve is the fitted line in the range of the $P_{\rm in}$.

of a large number of Ag NPs in the experiment than the simulation results only based on a single Ag NP model without considering plasmon coupling in order to simplify the computing process. Nevertheless, the predicted enhanced EM fields from the simulation are anticipated to significantly enhance the light absorption in the perovskite sensitizer layer and hence lead to improvement of photoresponsivity of the perovskite/graphene heterojunction photodetectors.

Perovskite CH3NH3PbI3 thin films were fabricated using a one-step spin-coating method (see Methods). Figure 5a displays the absorption spectrum of a 400 nm thick perovskite CH₃NH₃PbI₃ layer fabricated on glass. An absorption edge at around 780 nm is observed in the spectrum. At the incident wavelength of 585 nm, there is still ~20% incident transmitted through the perovskite layer. This is important to our experiment as the Ag NPs are at the bottom and the LSPR is only induced from the portion of transmitted light that is not absorbed by the perovskite layer in the devices without the Ag NP-silica metafilm substrate. Figure 5b compares the SEM images of perovskite films on the graphene/Si substrate (left) and on the graphene/Ag NPs-silica metafilm/Si substrate (right), respectively. From the SEM images of the perovskite film fabricated through a one-step spin-coating process, a wellcrystallized structure was observed. The difference of film morphology with and without the Ag NPs-silica metafilm is

Figure 5c illustrates the experimental setup for photoresponse measurement. Photodetectors were connected to an electrochemical workstation with light shining from the top of the devices. On the basis of the energy band alignment diagram at the perovskite CH₃NH₃PbI₃/graphene interface shown in Figure 5d, photogenerated holes will transfer from the perovskite to graphene upon light illumination, resulting in the so-called photogating effect by the trapped electrons in

perovskite at the interface. This leads to a change of the graphene channel conductivity as the photoresponse. 16 The hole doping of graphene because of hole transfer from perovskite to graphene has been confirmed in our previous studies of perovskite/graphene heterostructure photodetectors from the Dirac point shift toward positive gate voltages upon light illumination. 16,45

Figure 6a presents the dynamic photoresponse measured on perovskite/graphene heterojunction photodetectors with (black) and without (red) the plasmonic Ag NPs-silica metafilm substrate in response to 120 s light on and off (585 nm in wavelength and 1.27×10^{-6} W in power). For both devices, repeatable dynamic response patterns could be clearly observed, demonstrating the stable photodetection of the devices we fabricated. Figure 6b depicts the zoom-in view of one 60 s on/off response cycle measured under 585 nm illumination with power of 2.51×10^{-9} W. Remarkably, the photocurrent (or photoresponse) of the perovskite/graphene photodetector on the Ag NPs-silica metafilm is 7.45 times higher than its counterpart without the metafilm. Considering the two types of the devices would be otherwise identical except that one has the Ag NPs-silica metafilm substrate and the other does not, and the measurement was made under the same condition, the higher photocurrent in the device with the Ag NPs-silica metafilm substrate can be attributed to the LSPR enhancement of the light absorption by the perovskite film. Specifically, a factor of up to 7.45 enhancement in the photoresponse cannot be explained by the simple light reflection, which illustrates the importance in designing an efficient Ag NPs-silica metafilm for LSPR coupling by minimizing the loss mechanisms via charge, energy, and heat transfer. The rise times (time when 70% of the total response is reached 15,16,45,46) of perovskite photodetectors with and without Ag NPs are 7 and 9.8 s, respectively, which are

Table 1. Comparison of Responsivities and R Enhancement Factor with Early Reports Adopting the Strategy of Metal NPs in Perovskite Photodetectors and Photodetectors with Other Sensitizing Materials'

| device type | bias (V) | $P_{\rm in}$ (W) | R w/o NPs (A/W) | R w/ NPs (A/W) | R' w/o NPs (A/W) | R' w/ NPs (A/W) | R enhancement factor | refs |
|--|-------------|------------------------|--------------------|-------------------|----------------------|-----------------------|----------------------|--------------|
| perovskite + G + Au NPs | 0.1 | 1×10^{-8} | 10.4 | 20.4 | 10.4 | 20.4 | 1.96 | 29 |
| perovskite + Au nanorods | -1 | N/A | 200 | 317 | 20 | 31.7 | 1.59 | 30 |
| $MoS_2 + Ag NPs$ | 5 | 4.68×10^{-10} | 556 | 770 | 11.11 | 15.4 | 1.38 | 52 |
| ZnO nanowires + Ag NPs | 5 | 6×10^{-5} | 216 | 450 | 4.32 | 9 | 2.08 | 53 |
| 4H-SiC + Al NPs | 10 | 1.61×10^{-3} | 0.045 | 0.165 | 4.5×10^{-4} | 1.65×10^{-3} | 3.67 | 54 |
| perovskite + G + Ag NPs—silica metafilm | 0.1 | 2.51×10^{-9} | 66.44 | 495.3 | 66.44 | 495.3 | 7.45 | this work |

[&]quot;Responsivity R' refers to the photoresponsivity of these devices with the same bias voltage (0.1 V). The R enhancement factor is responsivity ratio of the devices with and without plasmonic metal NPs. G refers to graphene.

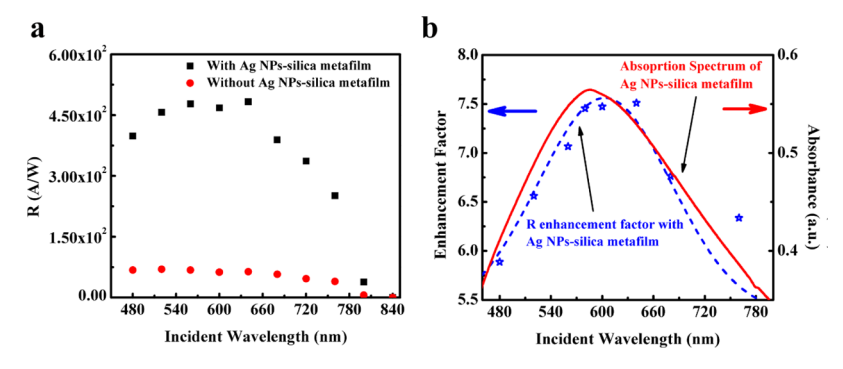


Figure 7. (a) Spectral photoresponsivity of the perovskite/graphene photodetectors with (black) and without (red) the Ag NPs-silica metafilm, Pin has a slightly variation from 1.42×10^{-9} to 4.60×10^{-9} W for different wavelength, bias = 0.1 V; (b) a comparison of the spectral photoresponsivity enhancement factor with a Ag NPs-silica metafilm (blue stars) and the absorption spectrum of the Ag NPs-silica metafilm (red); the blue dashed curve is the Gaussian fitting of spectral responsivity enhancement factor for the perovskite/graphene photodetectors with the Ag NPs-silica

comparable to the values reported in previously reported perovskite/graphene heterojunction photodetectors. 29,4 faster response in the photodetector on Ag NPs-silica metafilm substrate is because the extra absorption from the plasmonic enhanced field makes the photon-electron excitation saturate more rapidly. Also, slightly reduced fall time (time when 70% of the response is recovered) of the perovskite photodetector with Ag NPs was observed. This could be associated to less charge trapping at the graphene/ perovskite interface.

A comparison of the response time (rise time) of the devices on the Ag-silica metafilms is shown in Figure 6c under different incident light power. At the incident power of 1.27 μ W, the rise time of 0.6 s is comparable to that in early reports on perovskite photodetectors at similar light powers. 10,25,47 With decreasing light power, the response time decreases monotonically, which is consistent with prior observations. 48,49 At the incident light power of 2.51 nW as shown in Figure 6b, the time increases to 7 s. This behavior could be associated with the decay of transfer rate of electrons and/or holes from the light-absorbing materials to the conducting materials, especially in the case of a weak light signal.

Photoresponsivity is determined by the formula $R = I_{\rm ph}/P_{\rm in}$ where I_{ph} is the photocurrent and P_{in} is the power of incident light. Using this equation, the R values of the perovskite/ graphene photodetectors were calculated and the result is depicted as a function of the Pin (Figure 6d) for both perovskite/graphene photodetectors with (black) and without (red) the Ag NPs-silica metafilm substrate. In the P_{in} range of 1.27×10^{-6} to 2.51×10^{-9} W, the R values of both types of the photodetectors increase with decreasing P_{in} , which is

consistent with the previous reports and is attributed to increased probability of carrier recombination 45,50 at higher P_{in} . However, the R values of the photodetectors with the Ag NPs-silica metafilm substrate are consistently higher than that of its counterpart without the Ag NPs-silica metafilm substrate (Figure 6d). For example, the R values for the device without the Ag NPs-silica metafilm substrate are 4.25 and 66.44 A/W at the $P_{\rm in}$ of 1.27 × 10⁻⁶ and 2.51 × 10⁻⁹ W. In contrast, much higher R values of 10.3 and 495.3 A/W were obtained on the device with the Ag NPs-silica metafilm substrate with enhancement factors of 2.42 and 7.45, respectively, at these $P_{\rm in}$'s. Compared to the early works, which generally merged metal NPs in the active layer so the metal NPs are in a direct contact to perovskite film (Table 1), the 7.45 time enhancement is significantly higher and to our knowledge, the highest so far reported among devices adopting the plasmonic metal NPs in perovskite photodetectors. At 0.1 V of bias, the responsivity R' reaches 495 A/W, which is more than an order of magnitude higher than the prior reports of photodetectors with plasmonic metal NPs in perovskite. This result reveals that embedding the Ag NPs in thin silica films to prevent their contact with the perovskite (or active layer) is a crucial strategy to significantly enhance the performance of photodetectors by suppressing the energy and charge carrier loss as well as heat transfer to the perovskite film. Considering that the transmitted light is only about 20% of the incident light in this work because of the large thickness (~400 nm) of the perovskite films, higher enhancement factors are anticipated in sensitizer/graphene heterostructure photodetectors when the thickness of the sensitizer is significantly lower, such as a layer of nanocrystals of dimension in few to

tens of nanometers. Therefore, the Ag NPs-silica metafilm substrate can provide a promising LSPR scheme for many other devices, Moreover, as the responsivity enhancement from Ag NPs LSPR enhancement is more significant at lower light intensity, as indicated by the blue trendline of the enhancement factor with respect to P_{in} , this substrate may be particularly useful for photo detection at low-level light intensities.

Figure 7a displays the spectral responsivity of perovskite/ graphene heterojunction photodetectors with and without Ag NPs. The broad shoulder of the R value at 800-820 nm corresponds to the expected cut-off wavelength of perovskite at 785 nm (Figure 5a). Whereas enhanced R values in the perovskite/graphene heterojunction device on the Ag NPssilica metafilm substrate is observed across the whole visible region over its counterpart without such a substrate, the enhancement factor is not uniform, as displayed in Figure 7b, which has a good correspondence with the absorption spectrum of Ag NPs-silica metafilm in Figure 3c where we concluded that the LSPR of Ag NPs could be induced from a broadband incident light in the typical visible region. Thus, it further confirms the responsivity enhancement is primarily attributed to the near-field optical enhancement from LSPR of Ag NPs.

3. CONCLUSIONS

In this work, a low-cost and scalable metaplatform has been designed and synthesized for effective plasmon-exciton coupling for high-performance optoelectronic devices on top of such a metaplatform. Specifically, an in situ layer-by-layer deposition process was developed for coating of 10 nm thick silica on Ag NPs self-assembled on SiO₂/Si and glass substrates. The obtained Ag NP-silica metafilms are designed to provide effective light trapping around the Ag NPs through excitation of the localized surface plasmonic resonance, or LSPR, on Ag NPs. By embedding the Ag NPs in thin silica of an optimal thickness, the coupling of the evanescent LSPR field to optoelectronic devices and the suppression of the loss through transfer of energy, carrier and heat back to Ag NPs can be achieved, resulting in significant enhancement of optoelectronic performance. In addition, the precise placement of the Ag NP-silica metafilms under the active channel of the devices defined between electrodes was found important to avoid device failure through short circuits. As a proof of concept, organic-inorganic hybrid perovskite/graphene heterojunction photodetectors were fabricated on the Ag NP-silica metafilms and for investigation of the plasmon-exciton coupling. Hybrid perovskite thin film/graphene heterojunction photodetectors were fabricated on the Ag NP-silica metafilms with an enhancement factor of 7.45. To our knowledge, this enhancement factor is the highest so far among all the reports adopting the strategy of integrating NPs in perovskite photodetectors. Moreover, the Ag NPs-silica metafilm designed in this work could be adopted as a universal platform for improving the responsivity of 2D sensitizer/graphene heterojunction optoelectronics with other sensitizing materials such as QDs, organic molecules, and transition-metal dichalcogenide monolayers.

4. METHODS

4.1. Au Electrode Deposition. Device fabrication starts from Au electrode bars deposition on a SiO₂/Si substrate through a shadow mask using electron-beam evaporation. The dimension of each Au bar is 4 mm (length) × 1 mm (width), and the separation distance between neighboring Au bars is 1 mm, which defines the channel length after graphene is transferred across the two Au electrodes.

4.2. Ag NPs-Silica Metafilm Fabrication. The Ag NPs-silica metafilm substrate was fabricated in a three-step in situ process. First, an Ag thin film of nominal thickness of 8 nm was evaporated in the active device channel area between the two Au electrodes of a dimension of 4.0 mm (length) × 0.6 mm (width) defined using a shadow mask. Second, the Ag film was thermally annealed at 300 $^{\circ}C$ in high vacuum of 1 \times 10 $^{-6}$ Torr for 30 min to enable Ag NPs' selfassembly. Finally, a 10 nm thick SiO2 was evaporated on the Ag NPs using the same shadow mask. The evaporation of Ag and SiO2 was carried out at room temperature. Considering the instability of the metafilms under the thermal budgets required for fabrication of the perovskite/graphene photodetectors, the confinement of the Ag NPs-silica metafilm within the active device channel area was found critical to avoiding short-circuits of the devices caused by thermally driven metal diffusion from Ag NPs to the surface of the SiO₂

4.3. Perovskite/Graphene Heterojunction Photodetector Fabrication. Single-layer graphene was synthesized using chemical vapor deposition on commercial copper foils (Sigma-Aldrich, USA) at 1000 °C and then transferred onto the SiO₂/Si substrate with prefabricated Au electrodes. The details of graphene growth and transfer were reported in the previous work. 11,45,51

The perovskite film was fabricated on graphene using a one-step spin-coating method as explained in ref 45 Briefly, the CH₃NH₃PbI₃ precursor solution was prepared by dissolving the lead iodide, PbI₂ (Alfa Aesar, 99.9985%), and methylammonium iodide, MAI (Luminescence Technology, 99.5%) in dimethylformamide (DMF). Specifically, for this experiment, 0.69 g of PbI₂ and 0.24 g of MAI were dissolved in 2 mL of DMF to get a molar ratio of 1:1 (0.75 M each). The solution was stirred overnight at 1200 rpm and 70 °C. The precursor solution and the graphene substrate were preheated at 80 °C before device fabrication. The perovskite film was prepared by spin-coating the precursor at 500 rpm for 30 s, followed by a higher spin speed of 3000 rpm for 30 s in a nitrogen-filled glove box. Isopropyl alcohol was dispensed as an antisolvent during the spin in order to facilitate crystallization. The film was annealed at 70 °C for 20 min at 100 $^{\circ}\text{C}$ for 10 min to remove residual solvents.

4.4. Device Characterization. Absorption spectra were measured with a PerkinElmer Lambda 35 Spectrophotometer. SEM images were taken on a JEOL JSM-6380 scanning electron microscope. Raman spectra of the perovskite/graphene heterostructure were measured on a WiTec Alpha300 system with a 532 nm excitation laser. Dynamic photoresponses were recorded using a CH Instruments CHI660D electrochemical workstation connected by a homebuilt probe station, and the power of the incident light was measured using a Newport optical power meter.

ASSOCIATED CONTENT

S Supporting Information

The Supporting Information is available free of charge on the ACS Publications website at DOI: 10.1021/acsami.9b10706.

A failed attempt at integrating metal NPs in perovskite/ graphene photodetectors by placing Au NPs between graphene and the perovskite layer; noise power density and figure-of-merit detectivity (D^*) of the perovskite/ graphene photodetectors with and without the Ag NPssilica metafilm (PDF)

AUTHOR INFORMATION

Corresponding Authors

*E-mail: liubo@ku.edu (B.L.). *E-mail: jwu@ku.edu (J.Z.W.).

ORCID ®

Bo Liu: 0000-0003-0298-8238

Rithvik R. Gutha: 0000-0001-6172-2486 Mohammed Alamri: 0000-0002-7473-8644 Maogang Gong: 0000-0002-2031-781X Seyed M. Sadeghi: 0000-0002-5043-5032 Wai-Lun Chan: 0000-0001-8697-9894

Notes

The authors declare no competing financial interest.

ACKNOWLEDGMENTS

This research was supported in part by Army Research Office contract no. W911NF-16-1-0029, and US National Science Foundation contracts nos. NSF-DMR-1508494, NSF-ECCS-1809293, and NSF-DMR-1909292. The authors also acknowledge Liang Qin (University of Kansas, Beijing JiaoTong University) for his advice on preparing the perovskite films on graphene. W.-L.C. acknowledges the support by the US National Science Foundation grants NSF-DMR-1351716 and by the University of Kansas General Research Fund allocation #2151080.

REFERENCES

- (1) Green, M. A.; Ho-Baillie, A.; Snaith, H. J. The Emergence of Perovskite Solar Cells. *Nat. Photonics* **2014**, *8*, 506–514.
- (2) Grancini, G.; Roldan-Carmona, C.; Zimmermann, I.; Mosconi, E.; Lee, X.; Martineau, D.; Narbey, S.; Oswald, F.; De Angelis, F.; Graetzel, M.; Nazeeruddin, M. K. One-Year Stable Perovskite Solar Cells by 2D/3D Interface Engineering. *Nat. Commun.* **2017**, *8*, 15684.
- (3) Veldhuis, S. A.; Boix, P. P.; Yantara, N.; Li, M.; Sum, T. C.; Mathews, N.; Mhaisalkar, S. G. Perovskite Materials for Light-Emitting Diodes and Lasers. *Adv. Mater.* **2016**, *28*, 6804–6834.
- (4) Xiao, Z.; Kerner, R. A.; Zhao, L.; Tran, N. L.; Lee, K. M.; Koh, T.-W.; Scholes, G. D.; Rand, B. P. Efficient Perovskite Light-Emitting Diodes Featuring Nanometre-Sized Crystallites. *Nat. Photonics* **2017**, *11*, 108–115.
- (5) Zhao, Y.; Zhu, K. Organic-Inorganic Hybrid Lead Halide Perovskites for Optoelectronic and Electronic Applications. *Chem. Soc. Rev.* **2016**, *45*, 655–689.
- (6) Wang, H.; Kim, D. H. Perovskite-Based Photodetectors: Materials and Devices. *Chem. Soc. Rev.* **2017**, *46*, 5204–5236.
- (7) Mei, F.; Sun, D.; Mei, S.; Feng, J.; Zhou, Y.; Xu, J.; Xiao, X. Recent Progress in Perovskite-Based Photodetectors: The Design of Materials and Structures. *Adv. Phys.: X* **2019**, *4*, 1592709.
- (8) Park, N.-G. Perovskite Solar Cells: An Emerging Photovoltaic Technology. *Mater. Today* **2015**, *18*, 65–72.
- (9) Stranks, S. D.; Eperon, G. E.; Grancini, G.; Menelaou, C.; Alcocer, M. J. P.; Leijtens, T.; Herz, L. M.; Petrozza, A.; Snaith, H. J. Electron-Hole Diffusion Lengths Exceeding 1 Micrometer in an Organometal Trihalide Perovskite Absorber. *Science* **2013**, 342, 341–344.
- (10) Dang, V. Q.; Han, G.-S.; Trung, T. Q.; Duy, L. T.; Jin, Y.-U.; Hwang, B.-U.; Jung, H.-S.; Lee, N.-E. Methylammonium Lead Iodide Perovskite-Graphene Hybrid Channels in Flexible Broadband Phototransistors. *Carbon* **2016**, *105*, 353–361.
- (11) Gong, M.; Sakidja, R.; Goul, R.; Ewing, D.; Casper, M.; Stramel, A.; Elliot, A.; Wu, J. Z. High-Performance All-Inorganic CsPbCl₃ Perovskite Nanocrystal Photodetectors with Superior Stability. *ACS Nano* **2019**, *13*, 1772–1783.
- (12) Kwak, D.-H.; Lim, D.-H.; Ra, H.-S.; Ramasamy, P.; Lee, J.-S. High Performance Hybrid Graphene-CsPbBr₃-Xix Perovskite Nanocrystal Photodetector. *RSC Adv.* **2016**, *6*, 65252–65256.
- (13) Lee, Y.; Kwon, J.; Hwang, E.; Ra, C.-H.; Yoo, W. J.; Ahn, J.-H.; Park, J. H.; Cho, J. H. High-Performance Perovskite-Graphene Hybrid Photodetector. *Adv. Mater.* **2015**, *27*, 41–46.
- (14) Spina, M.; Lehmann, M.; Náfrádi, B.; Bernard, L.; Bonvin, E.; Gaál, R.; Magrez, A.; Forró, L.; Horváth, E. Microengineered

- CH₃NH₃PbI₃ Nanowire/Graphene Phototransistor for Low-Intensity Light Detection at Room Temperature. *Small* **2015**, *11*, 4824–4828.
- (15) Wang, Y.; Zhang, Y.; Lu, Y.; Xu, W.; Mu, H.; Chen, C.; Qiao, H.; Song, J.; Li, S.; Sun, B.; Cheng, Y.-B.; Bao, Q. Hybrid Graphene-Perovskite Phototransistors with Ultrahigh Responsivity and Gain. *Adv. Opt. Mater.* **2015**, *3*, 1389–1396.
- (16) Wu, L.; Qin, L.; Zhang, Y.; Alamri, M.; Gong, M.; Zhang, W.; Zhang, D.; Chan, W.-L.; Wu, J. Z. High-Sensitivity Light Detection Via Gate Tuning of Organometallic Perovskite/PCBM Bulk Heterojunctions on Ferroelectric Pb_{0.92}La_{0.08}Zr_{0.52}Ti_{0.48}O₃ Gated Graphene Field Effect Transistors. ACS Appl. Mater. Interfaces 2018, 10, 12824–12830.
- (17) Xia, H.-R.; Li, J.; Sun, W.-T.; Peng, L.-M. Organohalide Lead Perovskite Based Photodetectors with Much Enhanced Performance. *Chem. Commun.* **2014**, *50*, 13695–13697.
- (18) Liu, C.; Wang, K.; Yi, C.; Shi, X.; Du, P.; Smith, A. W.; Karim, A.; Gong, X. Ultrasensitive Solution-Processed Perovskite Hybrid Photodetectors. *J. Mater. Chem. C* **2015**, *3*, 6600–6606.
- (19) Hu, X.; Zhang, X.; Liang, L.; Bao, J.; Li, S.; Yang, W.; Xie, Y. High-Performance Flexible Broadband Photodetector Based on Organolead Halide Perovskite. *Adv. Funct. Mater.* **2014**, 24, 7373–7380
- (20) Eustis, S.; El-Sayed, M. A. Why Gold Nanoparticles Are More Precious Than Pretty Gold: Noble Metal Surface Plasmon Resonance and Its Enhancement of the Radiative and Nonradiative Properties of Nanocrystals of Different Shapes. *Chem. Soc. Rev.* **2006**, *35*, 209–217.
- (21) Cortie, M. B.; McDonagh, A. M. Synthesis and Optical Properties of Hybrid and Alloy Plasmonic Nanoparticles. *Chem. Rev.* **2011**, *111*, 3713–3735.
- (22) Xiao, X. H.; Ren, F.; Zhou, X. D.; Peng, T. C.; Wu, W.; Peng, X. N.; Yu, X. F.; Jiang, C. Z. Surface Plasmon-Enhanced Light Emission Using Silver Nanoparticles Embedded in ZnO. *Appl. Phys. Lett.* **2010**, 97, 071909.
- (23) Maier, S. A. Plasmonics: Fundamentals and Applications; Springer Science & Business Media, 2007; pp 65-87.
- (24) Willets, K. A.; Van Duyne, R. P. Localized Surface Plasmon Resonance Spectroscopy and Sensing. *Annu. Rev. Phys. Chem.* **2007**, 58, 267–297.
- (25) Wiederrecht, G. Handbook of Nanoscale Optics and Electronics; Academic Press, 2009; p 309.
- (26) Gutha, R. R.; Sadeghi, S. M.; Wing, W. J. Ultrahigh Refractive Index Sensitivity and Tunable Polarization Switching Via Infrared Plasmonic Lattice Modes. *Appl. Phys. Lett.* **2017**, *110*, 153103.
- (27) Gutha, R. R.; Sadeghi, S. M.; Hatef, A.; Sharp, C.; Lin, Y. Ultrahigh Refractive Index Sensitivity Via Lattice-Induced Meta-Dipole Modes in Flat Metallic Nanoantenna Arrays. *Appl. Phys. Lett.* **2018**, *112*, 223102.
- (28) Knight, M. W.; King, N. S.; Liu, L.; Everitt, H. O.; Nordlander, P.; Halas, N. J. Aluminum for Plasmonics. *ACS Nano* **2014**, *8*, 834–840.
- (29) Sun, Z.; Aigouy, L.; Chen, Z. Plasmonic-Enhanced Perovskite-Graphene Hybrid Photodetectors. *Nanoscale* **2016**, *8*, 7377–7383.
- (30) Wang, H.; Lim, J. W.; Quan, L. N.; Chung, K.; Jang, Y. J.; Ma, Y.; Kim, D. H. Perovskite-Gold Nanorod Hybrid Photodetector with High Responsivity and Low Driving Voltage. *Adv. Opt. Mater.* **2018**, *6*, 1701397.
- (31) Rai, P. Plasmonic Noble Metal@Metal Oxide Core—Shell Nanoparticles for Dye-Sensitized Solar Cell Applications. *Sustainable Energy Fuels* **2019**, *3*, 63–91.
- (32) Yip, C. T.; Liu, X.; Hou, Y.; Xie, W.; He, J.; Schlücker, S.; Dang Yuan Lei, D. Y.; Huang, H. Strong Competition between Electromagnetic Enhancement and Surface-Energy-Transfer Induced Quenching in Plasmonic Dye-Sensitized Solar Cells: A Generic yet Controllable Effect. *Nano Energy* **2016**, *26*, 297–304.
- (33) Liu, S.; Hou, Y.; Xie, W.; Schlucker, S.; Yan, F.; Lei, D. Y. Quantitative Determination of Contribution by Enhanced Local Electric Field, Antenna-Amplified Light Scattering, and Surface Energy Transfer to the Performance of Plasmonic Organic Solar Cells. *Small* **2018**, *14*, No. e1800870.

- (34) Boriskina, S. V.; Ghasemi, H.; Chen, G. Plasmonic Materials for Energy: From Physics to Applications. *Mater. Today* **2013**, *16*, 375–386
- (35) Divitini, G.; Cacovich, S.; Matteocci, F.; Cina, L.; Di Carlo, A.; Ducati, C. In Situ Observation of Heat-Induced Degradation of Perovskite Solar Cells. *Nat. Energy* **2016**, *1*, 15012.
- (36) Sadeghi, S. M.; Wing, W. J.; Gutha, R. R.; Sharp, C. Semiconductor Quantum Dot Super-Emitters: Spontaneous Emission Enhancement Combined with Suppression of Defect Environment Using Metal-Oxide Plasmonic Metafilms. *Nanotechnology* **2018**, *29*, 015402.
- (37) Sadeghi, S. M.; Wing, W. J.; Gutha, R. R.; Wilt, J. S.; Wu, J. Z. Balancing Silicon/Aluminum Oxide Junctions for Super-Plasmonic Emission Enhancement of Quantum Dots Via Plasmonic Metafilms. *Nanoscale* **2018**, *10*, 4825–4832.
- (38) Kato, Y.; Ono, L. K.; Lee, M. V.; Wang, S.; Raga, S. R.; Qi, Y. Silver Iodide Formation in Methyl Ammonium Lead Iodide Perovskite Solar Cells with Silver Top Electrodes. *Adv. Mater. Interfaces* **2015**, *2*, 1500195.
- (39) Xu, G.; Liu, J.; Wang, Q.; Hui, R.; Chen, Z.; Maroni, V. A.; Wu, J. Plasmonic Graphene Transparent Conductors. *Adv. Mater.* **2012**, 24, OP71.
- (40) Lee, K.-C.; Lin, S.-J.; Lin, C.-H.; Tsai, C.-S.; Lu, Y.-J. Size Effect of Ag Nanoparticles on Surface Plasmon Resonance. *Surf. Coat. Technol.* **2008**, 202, 5339–5342.
- (41) Eustis, S.; El-Sayed, M. A. Why Gold Nanoparticles Are More Precious Than Pretty Gold: Noble Metal Surface Plasmon Resonance and Its Enhancement of the Radiative and Nonradiative Properties of Nanocrystals of Different Shapes. *Chem. Soc. Rev.* **2006**, *35*, 209–217.
- (42) Ferrari, A. C.; Meyer, J. C.; Scardaci, V.; Casiraghi, C.; Lazzeri, M.; Mauri, F.; Piscanec, S.; Jiang, D.; Novoselov, K. S.; Roth, S.; Geim, A. K. Raman Spectrum of Graphene and Graphene Layers. *Phys. Rev. Lett.* **2006**, *97*, 187401.
- (43) Zhang, S.; Zhang, X.; Liu, X. Electromagnetic Enhancement of Graphene Raman Spectroscopy by Ordered and Size-Tunable Au Nanostructures. *Nanoscale Res. Lett.* **2015**, *10*, 390.
- (44) Lu, R.; Konzelmann, A.; Xu, F.; Gong, Y.; Liu, J.; Liu, Q.; Xin, M.; Hui, R.; Wu, J. Z. High Sensitivity Surface Enhanced Raman Spectroscopy of R6G on in Situ Fabricated Au Nanoparticle/ Graphene Plasmonic Substrates. *Carbon* **2015**, *86*, 78–85.
- (4\$) Qin, L.; Wu, L.; Kattel, B.; Li, C.; Zhang, Y.; Hou, Y.; Wu, J.; Chan, W.-L. Using Bulk Heterojunctions and Selective Electron Trapping to Enhance the Responsivity of Perovskite-Graphene Photodetectors. *Adv. Funct. Mater.* **2017**, *27*, 1704173.
- (46) Kim, S.; Menabde, S. G.; Jang, M. S. Efficient Photodoping of Graphene in Perovskite-Graphene Heterostructure. *Adv. Electron. Mater.* **2019**, *5*, 1800940.
- (47) Chang, P.-H.; Liu, S. Y.; Lan, Y. B.; Tsai, Y. C.; You, X. Q.; Li, C. S.; Huang, K. Y.; Chou, A. S.; Cheng, T. C.; Wang, J. K.; Wu, C. I. Ultrahigh Responsivity and Detectivity Graphene-Perovskite Hybrid Phototransistors by Sequential Vapor Deposition. *Sci. Rep.* **2017**, *7*, 46281.
- (48) Sarker, B. K.; Childres, I.; Cazalas, E.; Jovanovic, I.; Chen, Y. P. Gate-Tunable and High Responsivity Graphene Phototransistors on Undoped Semiconductor Substrates. arXiv preprint arXiv:1409.5725 2014.
- (49) Yan, F.; Li, J. H.; Mok, S. M. Highly Photosensitive Thin Film Transistors Based on a Composite of Poly(3-Hexylthiophene) and Titania Nanoparticles. *J. Appl. Phys.* **2009**, *106*, 074501.
- (50) Gong, M.; Liu, Q.; Cook, B.; Kattel, B.; Wang, T.; Chan, W.-L.; Ewing, D.; Casper, M.; Stramel, A.; Wu, J. Z. All-Printable Zno Quantum Dots/Graphene Van Der Waals Heterostructures for Ultrasensitive Detection of Ultraviolet Light. *ACS Nano* **2017**, *11*, 4114–4123.
- (51) Alamri, M.; Sakidja, R.; Goul, R.; Ghopry, S.; Wu, J. Z. Plasmonic Au Nanoparticles on 2D MoS₂/Graphene Van Der Waals Heterostructures for High-Sensitivity Surface-Enhanced Raman Spectroscopy. ACS Appl. Nano Mater. 2019, 2, 1412–1420.

- (52) Jing, W.; Ding, N.; Li, L.; Jiang, F.; Xiong, X.; Liu, N.; Zhai, T.; Gao, Y. Ag Nanoparticles Modified Large Area Monolayer MoS₂ Phototransistors with High Responsivity. *Opt. Express* **2017**, 25, 14565–14574.
- (53) Liu, Y.; Zhang, X.; Su, J.; Li, H.; Zhang, Q.; Gao, Y. Ag Nanoparticles@ZnO Nanowire Composite Arrays: An Absorption Enhanced UV Photodetector. *Opt. Express* **2014**, 22, 30148–30155.
- (54) Liu, S.-X.; Wang, T.; Chen, Z.-Z. High-Performance of Al Nanoparticle Enhanced 4H-SiC MSM Photodiodes for Deep Ultraviolet Detection. *IEEE Electron Device Lett.* **2017**, 38, 1405–1408